COMPARATIVE STUDY OF THE INDUCTANCES OF AN INDUCTION MOTOR WITH ROTOR ECCENTRICITIES

E. F. Rodriguez [1], J. A. Santisteban[1], A. C. Ferreira[2]
[1]Fluminense Federal University, PGMEC, Niterói – RJ, Brazil.
[2]Rio de Janeiro Federal University, COPPE – PEE, Rio de Janeiro – RJ, Brazil.
elkinrodvel@msn.com, jasantisteban@vm.uff.br and ferreira@coep.ufrj.br

***Abstract* – In this work, the inductances of an induction motor, which rotor may be misaligned, are evaluated. Two types of analysis are performed: Analytical Method (AM) and Finite Element Method (FEM). For radial displacements, both methods show equivalent results but to evaluate inductances as a function of angular displacements, only with FEM was possible to get results as with AM it would be necessary intricate functions. The inductances obtained with FEM were included in simulations of a bearingless induction motor with split windings. This approach shows a good agreement with experimental results.**

***Keywords* - Airgap Eccentricity, Bearingless Induction Motor, Finite Elements Method, Inductance.**

I. INTRODUCTION

Induction motors with split windings operating as bearingless induction motor are being studied since 1989 [1], [2] and [3]. With this configuration it is possible to generate torque and radial positioning forces. With this approach some works were reported in the literature focusing on starting and constant speed operation [4], [5]. Strategies of speed control with good responses were also reported in [6]. Respect to the implementation of controllers, a significative progress has been reported, including the use of DSP's. However, the effects of possible misalignment between rotor and stator were not considered.

With this in mind, the interaction between magnetic fluxes from induction motor when submitted to misalignment is being studied [7]-[8]. In [9], one interesting analytical method (AM) is presented. To study the effects of airgap misalignment, the surfaces of stator and rotor are approximated as cylinders.

In this work, the AM results are compared with simulations using the Finite Elements Method (FEM), which has been consolidated as an useful tool in the study of non-linear phenomena and of great complexity.

The aim is the study of the self and mutual inductances behavior of an induction motor when submitted to radial misalignment. These results will allow for the prediction of possible interferences of the magnetic fluxes inside the motor with the torque and radial forces. These concerns are present in the so called bearingless induction motor with split windings [10].

Manuscript received on 26/05/2010. Accepted for publication on 17/08/2010 by recommendation of the Editor João Onofre P. Pinto.

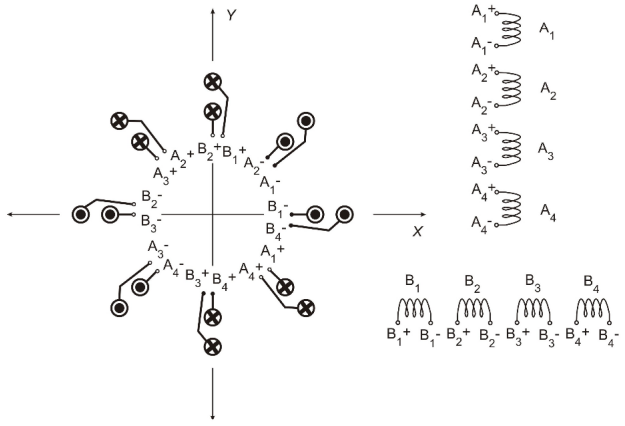

Fig. 1. Set of stator winding of the induction machine.

II. DETERMINATION OF MOTOR INDUCTANCES WITH NON UNIFORM AIRGAP

The machine analyzed in this work is a four poles, two phase induction motor, Figure 1. Each phase is composed of four windings that are connected in series in normal operation. When operating as a bearingless induction motor, each of the windings of one phase is supplied separately in order to control radial positioning. The other windings are connected in series and supplied simultaneously when is required the starting torque.

Table 1 shows the main parameters used to calculate inductances.

TABLE I
Parameters of biphase induction motor

External diameter of stator	122.00 mm
Internal diameter of stator	70.00 mm
Rotor diameter	68.00 mm
Airgap	1.00 mm
Length of the rotor	85.00 mm
Section area of the stator slot	85.71 mm^2
Area of the rotor slot	41.98 mm^2
Number of wires in each slot of the stator	25.00

A. Analytical Method (AM)

Assuming that the eccentricity of the rotor is limited to the airgap, it is possible to approximate the inverse of the airgap as the following function [9]:

$$P(\kappa) = \frac{1}{g(\kappa)} = \frac{1}{g_0}\sum_{i=0}^{\infty} P_i \cos\left[i(\kappa - \alpha)\right] \quad (1)$$

where κ is the reference angle of stator windings, α is the mechanical rotor displacement angle, g_0 is the uniform airgap, as shown in Figure 2, and

$$P_0 = \frac{1}{\sqrt{1-\varepsilon^2}}$$
$$P_i = 2P_0\left(\frac{1-\sqrt{1-\varepsilon^2}}{\varepsilon}\right)^i \quad (2)$$

where ε is the eccentricity between rotor and stator centers, calculated as:

$$\varepsilon = \frac{\sqrt{X_0^2 + Y_0^2}}{g_0} \quad (3)$$

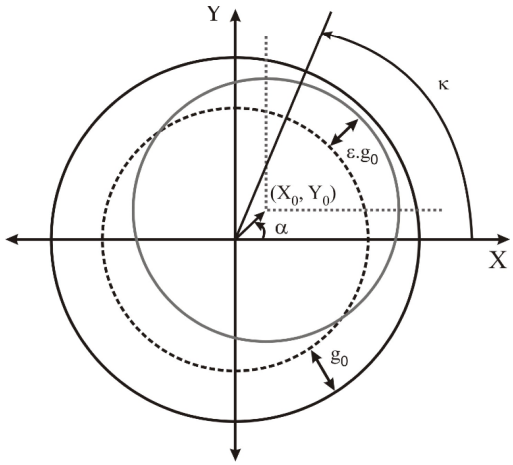

Fig. 2. Eccentricity of airgap.

Due to the magnetic field variation caused by the eccentricities of the airgap along any portion of winding *v*, it is possible to find

$$\int_{air-gap} \vec{H}_v(\kappa)\cdot d\vec{l} = n_v(\kappa)i_v \quad (4)$$

where H_v is the magnetic field intensity, n_v the turn function (number of coils), which depends of κ, and i_v is the winding current.

Manipulating (4) and (1), using Gauss law for magnetic fields in closed surfaces, assuming that the magnetic permeability of the core is infinite, that magnetic field is homogenous along the axial direction, that the dispersion of the magnetic field on both extremities of the rotor is neglected and considering that the airgap is very small when compared to the rotor radius, self and mutual inductances can be evaluated as in (5) and (6) respectively

$$L_{vv} = \frac{\lambda_{vv}}{i_v} = \mu_o rl\int_0^{2\pi} n_v(\kappa)N_v(\kappa)P(\kappa)d\kappa \quad (5)$$

$$L_{vw} = \frac{\lambda_{vw}}{i_w} = \mu_o rl\int_0^{2\pi} n_v(\kappa)N_w(\kappa)P(\kappa)d\kappa \quad (6)$$

where N_v and N_w are the winding functions. For instance, for winding *v*:

$$N_v = n_v - \frac{\int_0^{2\pi} n_v(k)P(k)dk}{\int_0^{2\pi} P(k)dk} \quad (7)$$

B. Finite Elements Method (FEM)

The complexity of the machine demands great care in its modeling through FEM. A three dimensional simulation would be more appropriate but it demands high computational effort. For this reason it was chosen a two dimensional simulation using an appropriated refinement on the mesh.

From electromagnetism the inductance can be expressed as:

$$L = \frac{N}{I}\Psi \quad (8)$$

where *L* is the inductance, *I* is the current, *N* is the number of turns and Ψ is the magnetic flux which can be obtained from (9).

$$\Psi = \int(\nabla \times \mathbf{A})\bullet d\mathbf{s} \quad (9)$$

According to *Stoke's* theorem and calculating the vector potential from its nodal values, it is possible to determine one relationship to calculate the inductance in a general form:

$$L = \frac{N}{I}\frac{l}{S}\sum_{i=1}^{m}\left(\frac{S_i}{n}\sum_{j=1}^{n} A_{ij}\right) \quad (10)$$

where *l* is the length of the rotor, A_{ij} the nodal vector potential, *S* is the total area in study, S_i the element area, *m* is the number of elements and *n* is the number of nodes by element (first-order triangle elements).

III. COMPARATIVE RESULTS

Inductance established through FEM (10) depends directly on the magnetic vector potential, which changes according to the rotor position. According to the AM these depend on (1).

In this work, self-inductances of phase A were evaluated using the AM and FEM. In Figures 3 and 4 are shown the self-inductances of windings A1 e A2 as a function of rotor horizontal displacements. The average errors are 8% approximately, which can be explained by the approximations used with the analytical method. This shows that FEM is a useful tool.

The results shown in Figures 5 and 6 would be difficult to be obtained with the analytical method. It is about the self-inductances of windings A1 and A2 when there are angular and radial displacements along the axis *x*. FEM shows that there is an important variation of self-inductances of winding A2 as the angular position of the rotor changes.

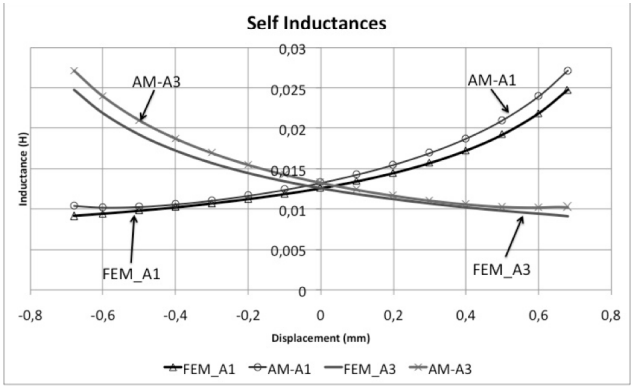

Fig. 3. Self-inductances of A1 and A3 windings submitted to radial displacements along the axis *x*.

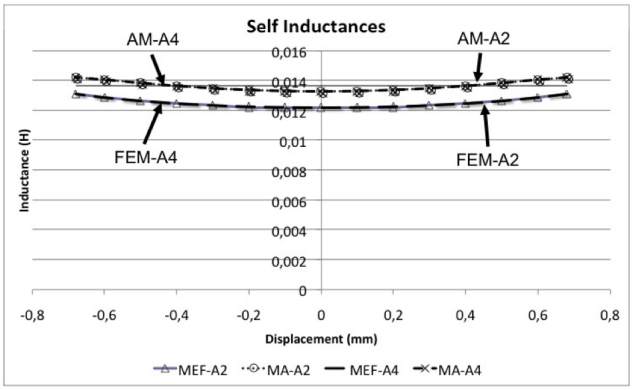

Fig. 4. Self-inductances of A2 and A4 windings submitted to radial displacements along the axis *x*

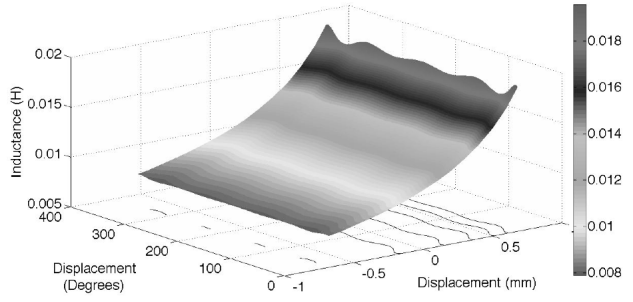

Fig. 5. Self-inductances of winding A1 submitted to angular and radial displacements along the axis *x*.

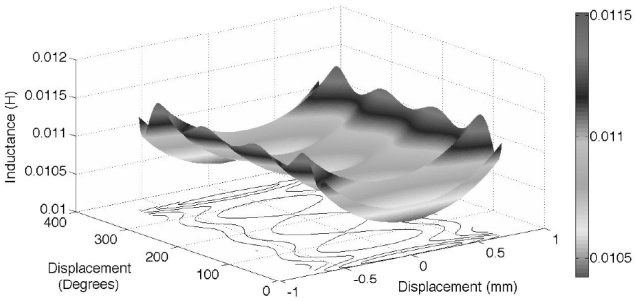

Fig. 6. Self-inductance of winding A2 submitted to angular and radial displacements along the axis *x*.

On the other hand, FEM shows that there is a strong influence of the angular displacement of the rotor in the mutual inductance between the stator and rotor, as seen in Figure 7.

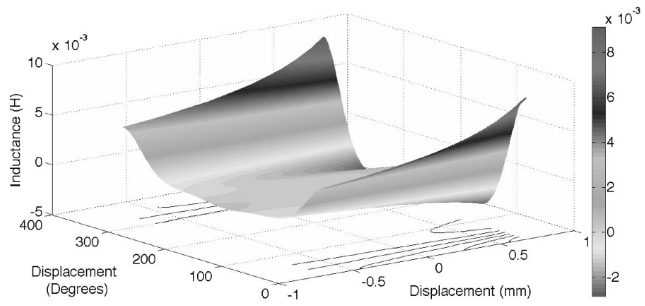

Fig. 7. Mutual inductance of winding A1 and the correspondent winding in the rotor submitted to angular and radial displacements along the axis *x*.

IV. DYNAMIC SIMULATIONS

In order to verify the effect of inductances variations, as calculated by FEM, in simultaneous speed and position closed loop control systems, the behavior of the motor under dynamic conditions was simulated using the software Matlab™. Figure 8 shows the block diagram of a combined conventional indirect airgap field oriented vector control with the radial position control for the bearingless induction motor. In this case, the speed controller is a proportional integral (PI) type. The reference flux is held constant and the PID radial position controllers generate the Δi_x and Δi_y current components according to the error between the position references and the position sensor signals. Related to the motor model, an inductances matrix $L(\theta,x)$, composed by all the values obtained through the FEM, was included. The simulations consider two conditions. In the first one, the rotor is arbitrarily unaligned 0.2mm along the axis x and the windings of phase A are activated in order to centralize the rotor. Details of the displacement control may be found in [11]. This process occurs during 0.6s. Figure 9 shows that the rotor is centralized in approximately 0.2s. On the other hand, Figure 10 shows the behavior of radial force, along the axis x. As noted, the force presents a ripple as the inductances are varying because of the rotor radial displacements. After 0.6s, the closed loop of speed vector control is initiated. Figures 9 and 10 show transient effects on both, radial displacement and force. Figure 11 shows the zoom of the rotor displacement. As observed, a vibration happens during all the starting. This result is in accordance with [10] and [12], where it was experimentally observed that the position controllers had not good performance when the motor was submitted to load torque. As seen in Figure 12, the net torque due to the vector control has a small ripple caused by the variations of inductances. This effect would not be foreseen if the analytical method to calculate the inductances were used. In Figure 13 the behavior of rotor speed after a step input of 900 rpm is shown.

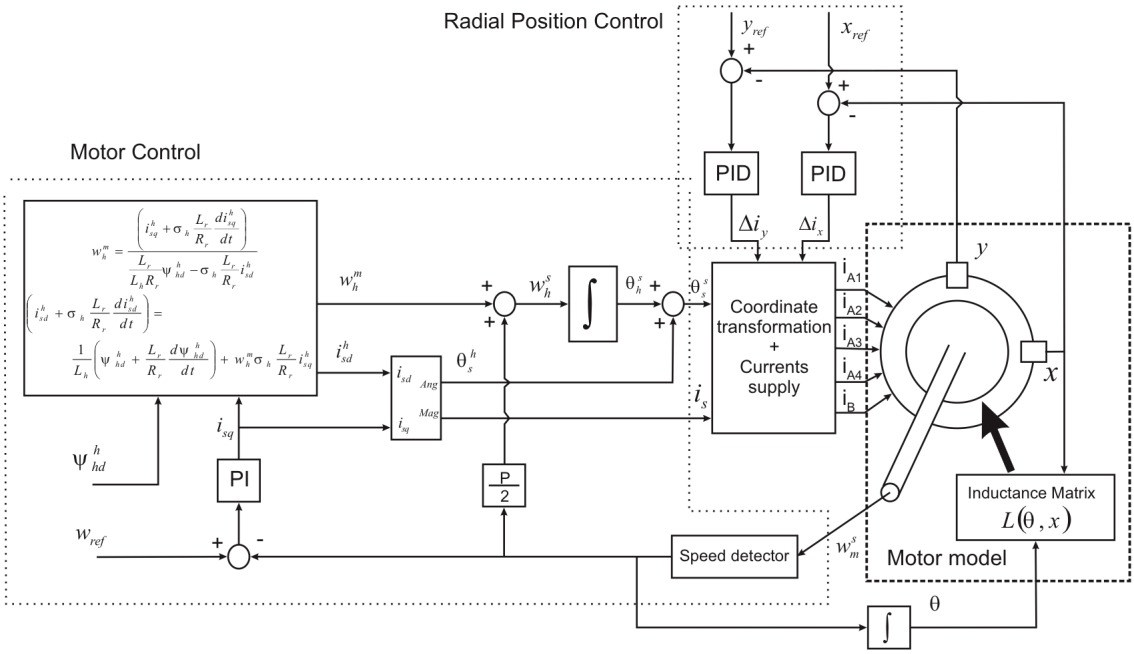

Fig. 8. Block diagram of an indirect airgap field oriented vector control for a bearingless induction motor with split windings.

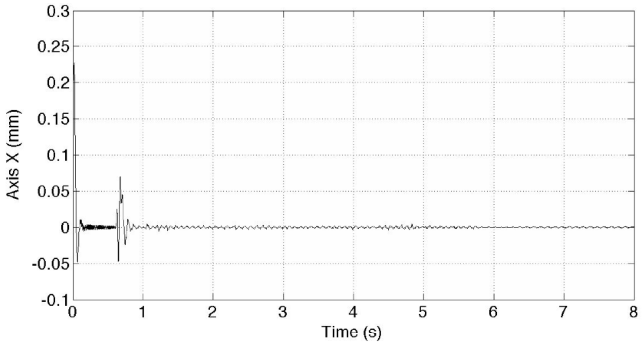

Fig. 9. Rotor radial displacement along the axis *x*.

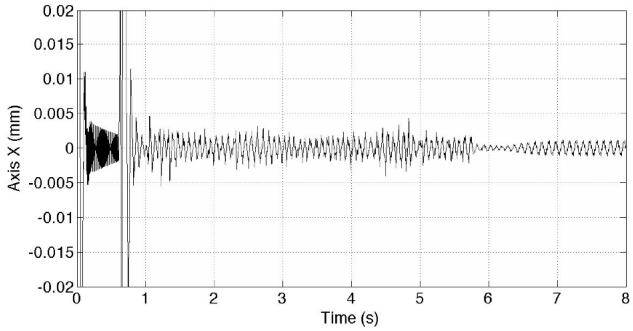

Fig. 11. Zoom of rotor displacement.

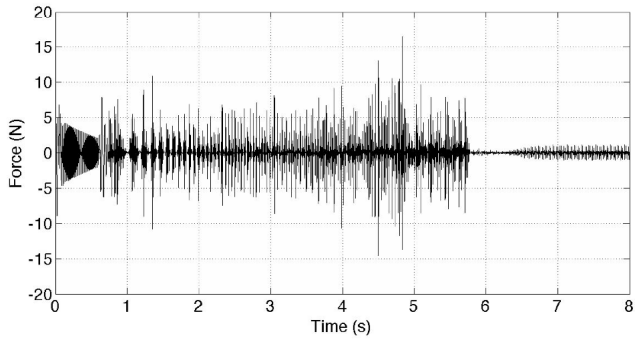

Fig. 10. Radial force along the axis *x*.

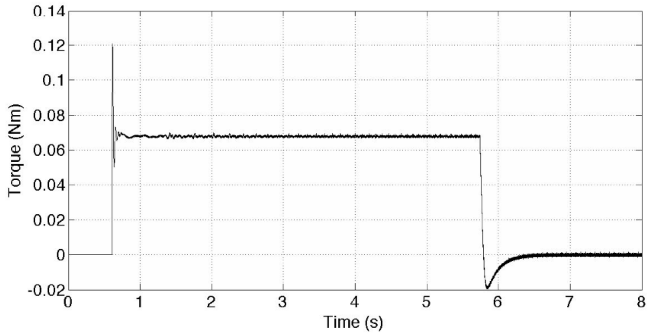

Fig. 12. Torque during the motor starting.

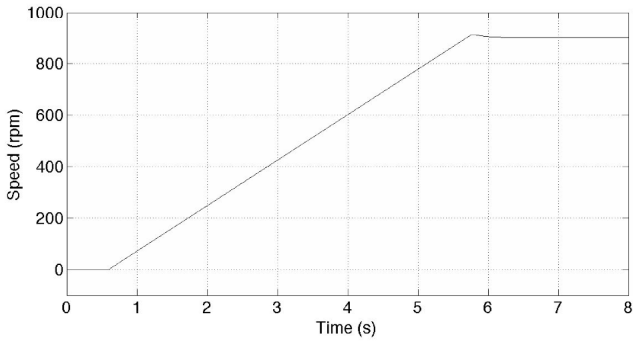

Fig. 13. Rotor speed.

In order to observe the effect of neglecting the inductance variations due to the angular displacements in the motor modeling, other simulations were performed. In this case, the inductance matrix was modified to set the inductance values as if the angular position were zero degrees so the inductances changes only by radial displacements.

Figures 14, 15 and 16 show the rotor displacement along the axis x, radial force and rotor speed, respectively. As seen, in the firsts 0.6s the behavior of rotor is the same of the previous case, because the same inductances were used. From 0.6s until 2s transient effects in the radial displacement and force are also observed. After 2s, the rotor suffers a constant and periodic vibration and the rotor reach a speed lower then the speed reference. Additionally, the simulation showed that the amplitude of stator current reached its maximum value, so this is the typical behavior of a detuned vector control. As seen in Figure 7, to neglect the dependence of angular displacement in mutual inductances between stator and rotor, even with the rotor centralized, implies an error into the value of the model parameters used in the vector control.

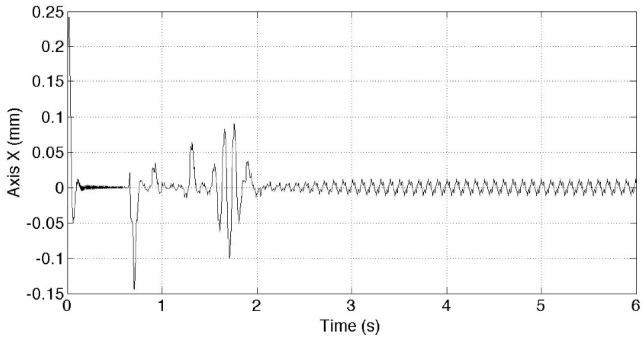

Fig. 14. Rotor displacement when the motor model uses an inductance matrix that does not depend on angular displacement.

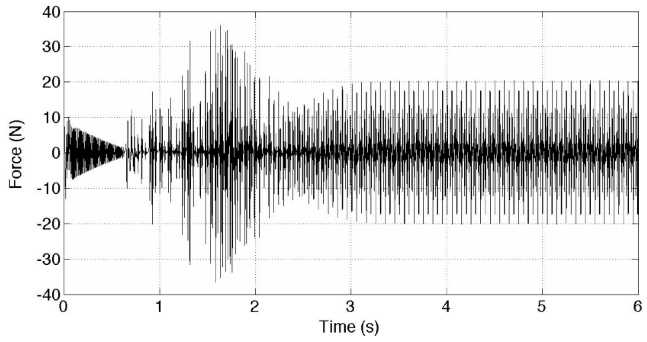

Fig. 15. Radial force.

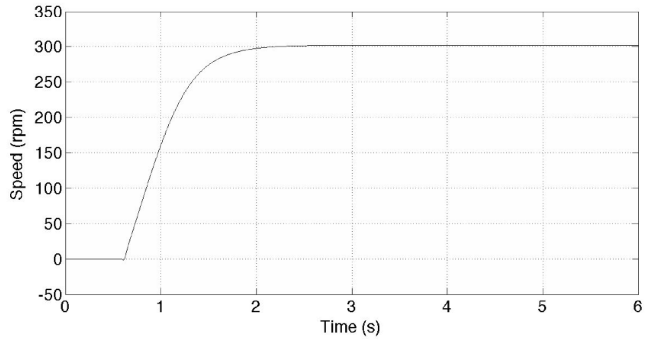

Fig. 16. Rotor speed.

V. EXPERIMENTAL RESULTS

In order to test the complete control system shown in Figure 8, a workbench was implemented. It consists of a low power bearingless induction motor with nominal airgap of 1mm, a current power supply module with five CC-VSI converters, a target desktop computer with A/D and D/A cards and a host computer running in the LabView environment. The target computer runs in a real time operative system. In Figure 17, the picture of the motor is shown.

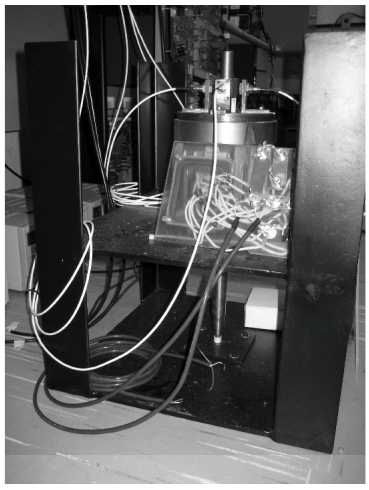

Fig. 17. The bearingless induction motor.

Using the same procedure as in the simulation, Figure 18 shows the behavior of rotor speed. After 1s, the closed loop speed control is activated and reaches the reference speed in approximately 8s.

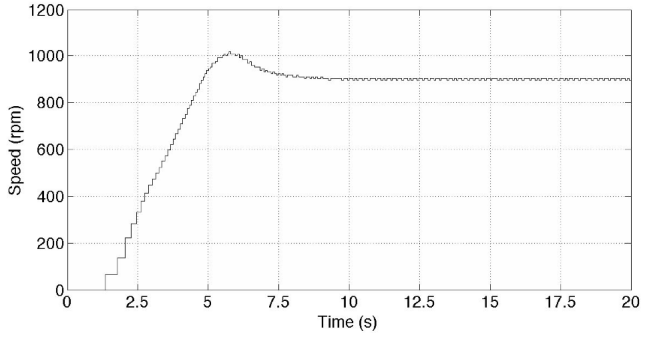

Fig. 18. Experimental rotor speed.

The radial displacement of the rotor along the x-axis is shown in Figure 19. In this case, after the activation of the speed control, a strong vibration happens during 2s. As noted, if compared with Figures 9 or 11, the transient and the vibrations are similar but the amplitudes and durations are different. This can be explained if it is taken into account that in the simulations the current power sources are ideal and the controllers are continuous. In the actual implementation the sources are half-bridge inverters and the controllers are digitally implemented.

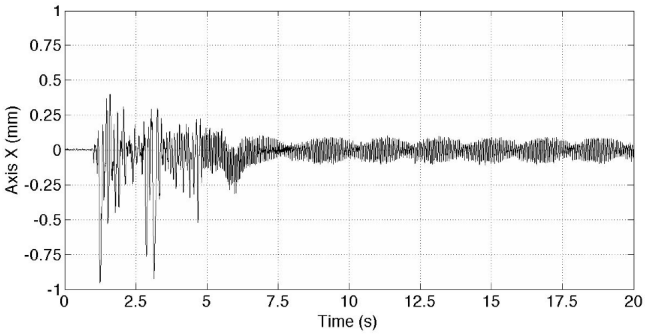

Fig. 19. Experimental radial displacement along the axis *x*.

VI. CONCLUSION

The reliability of finite elements method to calculate inductance variations on an induction motor with an unaligned rotor was tested. Some inductances would be very difficult to obtain using only analytical methods.

The importance of these results is related to the so called bearingless induction motor with split windings, where simultaneous torque and radial force are present. As previously noted, the displacement controller should be improved as the levels of rotor currents with a loaded motor affect the radial forces. FEM analysis shows that an additional consideration should be taken into account as some inductances are affected not only by the displacement but also by the angular position of the rotor and this determines directly the amplitude of torque harmonics.

Simulations using the motor model with inductances calculated by FEM show good agreement with experimental results.

ACKNOWLEDGEMENT

The authors would like to thank the financial support of CAPES, CNPq, PGMEC and Engineering school of UFF.

REFERENCES

[1] A. O. Salazar, and R. M. Stephan, “A Bearingless Method for Induction Machine”, *IEEE Transaction on Magnetics*, Vol. 29, No. 6, pp. 2965 – 2967, November 1993.

[2] A. O. Salazar, R. M. Stephan, and W. Dunford, "Mancais magnéticos para motores de indução utilizando os enrolamentos do estator", *VIII Congresso Brasileiro de Automática, Belém*, Vol. 2, pp. 930-935, Set. 1990.

[3] J. M. S. Ferreira, M. Zucca, A. O. Salazar and L. Donadio, “Analysis of a Bearingless Machine with Divided Windings”, *IEEE Transactions on Magnetics*, Vol. 41, No. 10, pp. 3931 – 3933, October 2005.

[4] R. R. Gomes, R. M. Stephan, and J. A. Santisteban, “Self-Bearing Motor with DSP Based Control System”, *X International Symposium on Magnetic Bearings*, Martigny, 2006.

[5] J. M. S. Ferreira, J. A. Paiva, A. O. Salazar, F. E. Castro, and S. N. D. Lisboa, “DSP Utilization in Radial Positioning Control of Bearingless Machine”, *ISIE – IEEE International Symposium on Industrial Electronics*, Vol. 1, pp. 312 – 317, 2003.

[6] J. A. Paiva, J. M. S. Ferreira, A. O. Salazar, and A. L. Maitelli, “Vectorial Speed Control using a Flux Estimator for Bearingless Machines with Divided Winding”, *The 10th Internation Symposium of Magnetic Bearing*, Aug. 21-23rd, Martigny, Switzerland, 2006.

[7] T. Tera, Y. Yamauch, A. Chiba, T. Fukao, and M. A. Rahman, “Performances of Bearingless and Sensorless Induction Motor Drive Based on Mutual Inductances and Rotor Displacements Estimation”, *IEEE Transactions on Industrial Electronics*, Vol. 53, No. 1, pp. 187 – 194, 2006.

[8] G. M. Joksimovic, “Dynamic Simulation of Cage Induction Machine with air gap eccentricity”, *IEE Proceedings – Electric Power Applications*, Vol. 152, No. 4, pp. 803 – 811, 2005.

[9] J. Faiz, and I. Tabatabaei, “Extension of Winding Function Theory for Nonuniform Air Gap in Electric Machinery”, *IEEE Transactions on Magnetics*, Vol. 38, No. 6, pp. 3654 – 3657, 2002.

[10] J. A. Santisteban, R. M. Stephan, “Analysis and Control of a Loaded Bearingless Machine”, *IEEE Transactions on Magnetics*, Vol. 35, No. 5, part 2, pp. 3998 – 4000, 1999.

[11] J. A. Santisteban, A. Ripper, R. M. Stephan, D. David and R. Noronha, “Controller Design for a Bearingless Electric Motor”, *Revista Brasileira de Ciências Mecânicas*, Volume XXI, Número 1, pp. 91-98, Março de 1999.

[12] J. A. Santisteban, R. M. Stephan, "Modelling and analysis of a loaded bearingless machine", *8th European Conference on Power Electronics and Applications EPE'99*, September 1999.

BIOGRAPHIES

Elkin F. Rodriguez V. was born in Bogotá, Colombia, in 1978. He received the Dipl.-Eng. degree in Electronic Engineering from "Los Libertadores" University, Bogotá, Colombia, in 2003. The M.Sc. degree in Mechanical Engineering from the Fluminense Federal University (UFF), in 2006, where he is currently working toward the D.Sc. degree. His main interests are control systems, instrumentation and electric machines.

José Andrés Santisteban, was born in Lima, Perú, 1961. He received the B.Sc. and the Engineer degrees in Electronic Engineering from Universidad Nacional de Ingeniería (UNI), Lima, Perú, in 1986 and 1988 respectively and the M.Sc and D.Sc. degrees in electrical engineering from Universidade Federal do Rio de Janeiro (COPPE/UFRJ), Brazil, in 1993 and 1999 respectively. From 1988 to 1991, he worked as a researcher and as an assistant professor in UNI. From 1993 to 1995 was a researcher at UFRJ. In 1999, he joined to Universidade Federal Fluminense, Niterói, Brazil, where he is currently an Associate Professor in the Electrical Engineering Department and the Post-graduate Program in Mechanical Engineering. He was an invited Associate Professor in Tokyo University of Science in 2003. His current research activities include bearingless machines, power electronics and electrical drives. Dr. Santisteban is member of IEEE and SOBRAEP (The Brazilian Society of Power Electronics).

Antonio Carlos Ferreira received the B.Sc. and M.Sc. degrees from the Federal University of Rio de Janeiro, Rio de Janeiro, Brazil, in 1987 and 1991, respectively, and the Ph.D. degree from the University of Cambridge, Cambridge, U.K., in 1997, all in Electrical Engineering. Since 1989, he has been with the Graduate School of Engineering, Federal University of Rio de Janeiro, where he is currently an Associate Professor, teaching at both under-graduate and post-graduate levels. His main interests are power system and electrical machines.